1 **SMAD4 promotes somatic-germline contact during murine oocyte growth**

2 Sofia Granados-Aparici[1,3,4,5], Qin Yang[1] and Hugh Clarke[1,2,3]

3 [1] Research Institute, McGill University Health Centre, 1001 Boul. Décarie, Montréal, QC, Canada H4A 3J1

4 [2] Departments of Obstetrics and Gynecology and Biology, Division of Experimental Medicine, McGill

5 University

6 [3] Corresponding authors (sograap@gmail.com; hugh.clarke@mcgill.ca)

7 [4] Cancer CIBER (CIBERONC), Madrid.

8 [5] Pathology Department, Medical School, University of Valencia-INCLIVA, Valencia.

9

10

11

Abstract

Development of the mammalian oocyte requires physical contact with the surrounding granulosa cells of the follicle, which provide it with essential nutrients and regulatory signals. This contact is achieved through specialized filopodia, termed transzonal projections (TZPs), that extend from the granulosa cells to the oocyte surface. Transforming growth factor (TGFβ) family ligands produced by the oocyte increase the number of TZPs, but how they do so is unknown. Using an inducible Cre recombinase strategy together with expression of green fluorescent protein to verify Cre activity in individual granulosa cells, we examined the effect of depleting the canonical TGFβ mediator, SMAD4. We observed a 20-50% decrease in the total number of TZPs in SMAD4-depleted granulosa cell-oocyte complexes, and a 50% decrease in the number of newly generated TZPs when the granulosa cells were reaggregated with granulosa cell-free wild-type oocytes. Three-dimensional image analysis revealed that TZPs of SMAD4-depleted cells were also longer than controls and more frequently oriented towards the oocyte. Strikingly, the transmembrane proteins, N-cadherin and Notch2, were reduced by 50% in these cells. SMAD4 may thus modulate a network of cell adhesion proteins that stabilize the attachment of TZPs to the oocyte, thereby amplifying signalling between the two cell types.

Impact statement

Genetic deletion of SMAD4 in the granulosa cells of growing ovarian follicles reduces the number of transzonal projections that contact the oocyte, implicating TGFβ-family signaling in maintaining soma-germ line communication.

Key words

SMAD / oocyte / TZPs / filopodia / follicle / signalling

33 **Introduction**

34 The development of a healthy oocyte within the ovarian follicle requires continuing contact between the
35 germ cell and the somatic granulosa cells that surround it (El-Hayek and Clarke, 2016, Clarke, 2018, Richani
36 et al., 2021, Robert, 2021, Li and Albertini, 2013, Doherty et al., 2022, Xie et al., 2023, Marchais et al.,
37 2022). Signals from the granulosa cells initiate the increase in volume of the oocyte when primordial (non-
38 growing) follicles are activated to enter the growth phase (Zhang et al., 2014, Saatcioglu et al., 2016,
39 Nagamatsu et al., 2019). Subsequently, the granulosa cells provide nucleotides, amino acids and pyruvate
40 to the growing oocyte via gap junctions that connect the two cell types (Xie et al., 2023, Clarke, 2018,
41 Marchais et al., 2022). When gap junctional communication between the two cell types is genetically
42 disrupted, oocytes do not develop normally and cannot be fertilized (Gittens and Kidder, 2005, Simon et
43 al., 1997, Winterhager and Kidder, 2015, Carabatsos et al., 2000). Once the oocyte reaches full-size, it
44 acquires the ability to undergo the final stage of development, termed meiotic maturation, but is
45 prevented from precociously doing so by cyclic GMP that is produced and transferred to it by the
46 granulosa cells, also via gap junctions (Jaffe and Egbert, 2016, Wigglesworth et al., 2013, Norris et al.,
47 2009, Zhang et al., 2010). In vitro, oocytes can develop normally when enclosed by granulosa cells but not
48 when the granulosa cells are removed and provided in co-culture, further emphasizing the crucial
49 importance of physical contact between the two cell types (O'Brien et al., 2003, Eppig, 1979, Herta et al.,
50 2021).

51 In primordial follicles, a single layer of squamous granulosa cells surrounds the oocyte and contact it via
52 adherens junctions (Mora et al., 2012, Jorgensen, 2013). Following activation of growth, a glycoprotein-
53 rich coat termed the zona pellucida becomes established around the oocyte (Litscher and Wassarman,
54 2020, Wassarman and Litscher, 2018). The zona pellucida steadily thickens as growth continues, reaching
55 a final thickness of about 7 µm in mice and 15 µm in humans. Despite the barrier imposed by the zona

56 pellucida, the granulosa cells and oocyte maintain direct contact by a dense network of thin filopodia-like
57 projections, termed transzonal projections (TZPs), that grow out from the granulosa cells through the zona
58 pellucida (Clarke, 2022, Macaulay et al., 2014, Baena and Terasaki, 2019, Motta et al., 1994, Zhang et al.,
59 2021, Albertini and Rider, 1994). The tips of the TZPs establish contact with the oocyte plasma membrane
60 through heterotypic adherens junctions comprising N-cadherin (granulosa cell) and E-cadherin (oocyte)
61 and harbour the gap junctions that link the two cell types (Mora et al., 2012) and likely also through focal
62 adhesions (McGinnis and Kinsey, 2015). New TZPs are generated throughout follicular growth, thereby
63 increasing intercellular molecular trafficking (El-Hayek et al., 2018a). A genetically imposed decrease in
64 the number of TZPs leads to defects in oocyte gene expression and to abnormal meiotic maturation and
65 embryonic development (Crozet et al., 2023). Despite the essential role of TZPs during oocyte
66 development in mammals, as well as the presence of analogous structures in non-mammalian species
67 (Kessel et al., 1985, Schroeder, 1981), the molecular mechanisms that govern their generation and
68 stability are not yet understood.

69 The TGFβ signalling pathway regulates the functions and interactions of a wide range of cell types under
70 various physiological and pathological conditions (Derynck and Budi, 2019, Peng et al., 2022). Binding of
71 the ligand to a complex of type I and type II receptors located at the cell surface activates signalling within
72 the cell, most commonly through the members of the SMAD family of transcription factors, although
73 SMAD-independent signaling can also occur (Aashaq et al., 2022, Derynck and Budi, 2019). Upon
74 phosphorylation of the tetrameric type II and type I receptors and subsequent phosphorylation of
75 receptor-activated SMAD proteins (R-SMADs; SMAD1, 2, 3, 5 and 8), a heterotrimeric complex with
76 SMAD4 is formed which enters the nucleus and regulates gene expression by binding to specific SMAD-
77 binding DNA elements. Although R-SMADs can signal in the absence of SMAD4, evidence indicates that
78 the presence of SMAD4 in the heterotrimer amplifies TGFβ cell signalling by stabilizing the complex and

79 by favouring the binding of other transcriptional co-repressors or co-activators of target genes (Aragón et
80 al., 2019, Guglielmi et al., 2021).

81 Genetic, pharmacological and in vitro studies have revealed multiple roles for TGFβ/SMAD signaling
82 during follicular growth and development (Patton et al., 2021, Pangas and Rajkovic, 2015). TGFβ signalling
83 via SMAD3 in granulosa cells acts initially in primordial follicles to maintain their quiescence (Granados-
84 Aparici *et al*, 2019; Wang *et al*, 2014) and later, following their activation, becomes excluded from the
85 nucleus in association with rapid granulosa cell growth and proliferation (Hardy *et al*, 2018). The TGFβ
86 superfamily members, growth-differentiation factor (GDF) 9, which signals through SMAD2/3, and bone
87 morphogenetic protein (BMP) 15, which signals through SMAD1/5/8, are produced by the oocyte (Dong
88 et al., 1996, Yan et al., 2001). Female mice lacking GDF9 rarely generate more than a single layer of
89 granulosa cells (Elvin et al., 1999a, Elvin et al., 1999b, Dong et al., 1996). This defect can be rescued by
90 preventing the production of inhibin, and the doubly mutant follicles can develop at least to the pre-antral
91 stage (Wu et al., 2004). Genetic inactivation of SMAD4 in the granulosa cells from growing follicles leads
92 to a reduction in the number of antral follicles and ovulated eggs, as well as the appearance of luteinized
93 follicles containing entrapped oocytes (Pangas et al., 2006). Similar phenotypes are observed when both
94 SMAD2 and SMAD3 are inactivated in the granulosa cells (Li et al., 2008). These effects are likely due at
95 least in part to a failure of the cumulus layer to expand in response to the ovulatory surge of LH (Pangas
96 et al., 2006, Li et al., 2008), as expansion is known to require SMAD signaling and to be required for
97 ovulation (Dragovic et al., 2007, Hao et al., 2022, Mottershead et al., 2015, Peng et al., 2013, Yu et al.,
98 2013).

99 Two lines of evidence point to a potential role for SMAD signaling in the generation or maintenance of
100 TZPs. First, deletion of GDF9 leads to both a decrease in the number of TZPs and a failure of a proportion
101 of the TZPs to correctly orient towards the oocyte (Carabatsos et al., 1998). Second, TZP number is

102 reduced in follicles grown in vitro following RNAi-mediated depletion of GDF9 in the oocyte (El-Hayek et
103 al., 2018a). To test the role of SMAD4 specifically, we used a Cre-lox strategy to inactivate *Smad4* in
104 granulosa cells, through expression of the recombinase under the control of the *Amhr2* (anti-Mullerian
105 hormone receptor 2) promoter, as previously described (Jorgez et al., 2004, Pangas et al., 2006). Using
106 image analysis tools and three-dimensional reconstructions, we show that depletion of SMAD4 in the
107 granulosa cells decreases the number of TZPs that project from individual granulosa cells in both intact
108 granulosa cell-oocyte complexes (GOCs) and in reaggregated complexes. Morphometric parameters
109 including length and orientation are also altered. The decrease in TZP number in intact GOCs is associated
110 with a reduction in the amount of N-cadherin and Notch2 in the granulosa cells, suggesting that the
111 composition of the granulosa cell surface is perturbed in the absence of SMAD4. We propose that SMAD4,
112 through its activity to increase expression of target genes, stabilizes TZPs by promoting their adhesion to
113 the oocyte surface, thereby helping to increase the number of TZPs and communication between the
114 growing oocyte and its follicular microenvironment.

115

116 **Results**

117 We began by verifying the expression of SMAD4 during folliculogenesis. As shown in Fig. 1A and consistent
118 with prior reports, SMAD4 was detectable in primordial and growing follicles as well as in the granulosa
119 cells collected from pre-antral follicles. SMAD2 and SMAD3 were also present, with SMAD2 being the
120 major species detected in oocytes. Two strategies were tested to deplete SMAD4 from the granulosa cells
121 of growing follicles. First, mice were generated carrying two floxed *Smad4* alleles and a transgene
122 encoding Cre recombinase under the control of the *Amhr2* promoter (Fig. 1B). These mice also carried a
123 transgene (*mTmG*, see Methods) constructed such that Tomato fluorescent protein is expressed in the
124 absence of Cre activity, whereas Cre-mediated recombination switches expression to green fluorescent

125 protein (GFP), thus allowing us to identify cells where Cre had been active. Upon immunostaining of
126 ovarian sections or whole-mount intact follicles, only a small number of cells expressed GFP (Fig. 1C, left).
127 Consistent with this observation, less than 10% of FACS-sorted granulosa cells were GFP-positive (Fig. 1C,
128 right). Thus, in our system, *Amhr2-Cre* did not mediate efficient recombination of floxed DNA in granulosa
129 cells. This is consistent with results described in previous reports (Pangas et al., 2006, Li et al., 2008).

130 We therefore turned to mice that expressed Cre under the control of a tamoxifen-inducible form of the
131 estrogen receptor (ER) gene promoter (*ER-Cre*). Because ER is expressed in pituitary gonadotropes and
132 SMAD4 regulates the transcription of the *Fshb* gene encoding the β-subunit of follicle-stimulating
133 hormone (Li et al., 2018), this model could not be used in vivo. Granulosa cell-oocyte complexes (GOCs)
134 from mid-growth stage follicles (diameter 100-120 µm) were therefore isolated, exposed to tamoxifen for
135 one day and then incubated in tamoxifen-free medium for another five days. Under these conditions, a
136 substantial fraction of the granulosa cells underwent Cre-mediated recombination, as indicated by the
137 expression of GFP in immunostained GOCs and by FACS analysis (Fig. 1E). This in vitro system was used
138 for the experiments described here.

139 To examine the efficiency of Cre-mediated *Smad4* recombination, the mRNA level was assessed in intact
140 GOCs using the RNAscope technique and in purified granulosa cells using qRT-PCR. Following tamoxifen
141 treatment and culture, there was an approximately 60% reduction in the number of foci in the granulosa
142 cells from 5.78 +/- 0.36 (mean, s.e.m., n=21) in *ER-Cre*$^{-}$; *Smad4*$^{fl/fl}$ mice to 2.16 +/- 0.26 (n=26) in *ER-Cre*$^{+}$;
143 *Smad4*$^{fl/fl}$ mice (p<0.0001), and a 70% reduction in the amount of PCR product from granulosa cells (n=5,
144 p=0.0001) (Fig. 1F). Immunoblotting of granulosa cells revealed a corresponding 70% reduction in SMAD4
145 protein in the granulosa cells of *ER-Cre*$^{+}$; *Smad4*$^{fl/fl}$ mice compared to *ER-Cre*$^{-}$; *Smad4*$^{fl/fl}$ controls (n=11,
146 p<0.0001) (Fig. 1G). Thus, the in vitro ER-Cre strategy substantially reduced although did not eliminate
147 SMAD4 from the granulosa cells.

148 To examine the effect of SMAD4 depletion on the TZPs, GOCs were isolated and cultured as above, fixed
149 and stained using anti-GFP to label cells where Cre had been active and phalloidin to label the TZPs, and
150 imaged them using confocal microscopy. First, the TZPs were analyzed as a population. Because TZPs arise
151 from both the innermost and more distal granulosa cell layers (Baena and Terasaki, 2019), it was not
152 possible to reliably determine how many granulosa cells contributed the GFP-positive TZPs in a GOC. The
153 total number of phalloidin-stained TZPs – irrespective of whether they were GFP-positive – that projected
154 to the oocyte in equatorial optical sections of GOCs from control (*Smad4*$^{wt/wt}$) and experimental (*Smad4*$^{fl/fl}$)
155 mice were therefore counted (Fig. 2A, B). TZP-number was normalized to the diameter of the
156 corresponding oocyte, although the mean oocyte diameter did not differ between the groups (Fig. 2B),
157 We observed a 20.4 +/- 0.05% reduction in the number of TZPs in the GOCs from the *Smad4*$^{fl/fl}$ mice (n=63
158 [control], 59 [experimental], p=0.002).

159 A limitation of quantifying TZPs in intact GOCs is that the granulosa cells, depending on their number and
160 spatial distribution, can variably impair their resolution and discrimination even using confocal
161 microscopy. Therefore, the number of TZPs was also counted after mechanically removing the granulosa
162 cells from the GOCs. This analysis revealed a striking 51.1 +/- 0.04% reduction in the normalized number
163 of TZPs in the GOCs from the *Smad4*$^{fl/fl}$ mice (n=44 [control], 47 [experimental], p<0.0001) (Fig. 2C, D). As
164 observed using intact GOCs, the mean oocyte diameter did not differ (Fig. 2D). To verify the difference in
165 TZP-number, we also compared *ER-Cre*$^{+}$; *Smad4*$^{fl/fl}$ to a different control genotype, *ER-Cre*$^{-}$; *Smad4*$^{fl/fl}$ mice.
166 A quantitatively similar 43.6 +/- 0.04% decrease in TZPs within the *ER-Cre*$^{+}$ population (n=164 [control],
167 172 [experimental], p<0.0001) (Fig. 2D) was observed following tamoxifen treatment and culture.
168 Together, these results indicate that depletion of SMAD4 in the granulosa cells is associated with a
169 decrease in the number of TZPs.

170 TZPs provide the physical platform that enables essential gap junctional communication between the
171 granulosa cells and the oocyte. To test whether the reduction in TZP number in SMAD4-depleted
172 granulosa cells impaired this communication, we used a fluorescence recovery after photobleaching
173 (FRAP) assay. Control and experimental GOCs were treated with tamoxifen and incubated as above. After
174 five days, they were exposed to calcein-AM, a fluorescent dye that can pass through gap junctions. The
175 fluorescence in the oocyte of each GOC was bleached using the laser of a confocal microscope and its
176 recovery was then recorded. As shown in Fig. 2E, which plots the fluorescence in the oocyte as a function
177 of time after photobleaching and at the end of the recording period normalized to the initial fluorescence,
178 we observed no difference between groups in the rate of transfer of fluorescence from the granulosa cells
179 to the oocyte. Thus, despite the decreased number of TZPs, depletion of SMAD4 did not detectably impair
180 gap junctional communication between the granulosa cells and the oocyte.

181 As TZPs project not only from the cells immediately adjacent to the zona pellucida but also from those in
182 more distal layers, it was possible that the reduced number of TZPs in *ER-Cre*$^{+}$; *Smad4*$^{fl/fl}$ complexes
183 reflected an impaired ability of the granulosa cells to proliferate. *ER-Cre*$^{+}$*; Smad4*$^{+/+}$ and *ER-Cre*$^{+}$*; Smad4*$^{fl/fl}$
184 GOCs were incubated for 5 hr in the presence of the thymidine analogue, EdU, added five days after the
185 tamoxifen exposure. No difference between the groups in the fraction of EdU-positive cells was observed
186 (Fig. 2F), however, implying that the reduced number of TZPs was not due to impaired proliferation of the
187 granulosa cells.

188 We then focused our analysis on individual granulosa cells. GOCs where individual GFP-positive cells could
189 be readily identified and the TZPs were easily attributable to a particular cell (Fig. 3A) were selected, serial
190 optical sections were obtained using confocal microscopy, and 3-dimensional images were reconstructed
191 using Imaris software. Fig. 3B shows one such reconstruction, where GFP-positive granulosa cells are
192 pseudo-coloured in green. We observed a 25% decrease in the mean volume of *Smad4*$^{fl/fl}$ granulosa cells

193 compared to wild-type cells (323.2 +/- 11.2 vs 242.6 +/- 10.0; n=293, 322; $p<0.0001$), but no difference
194 between genotypes in the sphericity of the cells (Fig. 3C). The TZPs in a subset of the GFP-positive
195 granulosa cells were then analyzed (Fig. 3D). In this subset, there was a 15% difference in mean cell volume
196 (392.2 +/- 20.8 vs 334.0 +/- 21.2; n=55, 63) which did not reach statistical significance ($p=0.054$). However,
197 whereas wild-type cells harbored a mean of 15.8 +/- 0.87 (n=55) TZPs per cell, this number was reduced
198 by 35% in *Smad4*$^{fl/fl}$ cells to 10.5 +/- 0.71 (n=65, $p<0.0001$). As compared to those of wild-type cells, the
199 TZPs of the *Smad4*$^{fl/fl}$ cells were about 10% longer (4.64 +/- 0.08 µm vs 5.19 +/- 0.09 µm; n=893, 720;
200 $p<0.0001$) and very slightly narrower (0.40 +/- 0.003 µm vs 0.38 +/- 0.003 µm; n=870, 719; $p<0.0001$)(Fig.
201 3E). We did not detect other differences between the genotypes in TZP morphology. These results
202 obtained using reconstructed 3-dimensional images of GFP-positive cells establish that the number of
203 TZPs is reduced in individual SMAD4-depleted granulosa cells.

204 A limitation of analyzing TZPs in GFP-positive cells within GOCs is that that this strategy cannot distinguish
205 TZPs that were generated in a low-SMAD4 environment (i.e., after the Cre recombinase was expressed)
206 from those generated earlier in a normal-SMAD4 environment. To ensure that we examined only TZPs
207 that were generated after Cre had been expressed, we used our previously published reaggregation assay
208 (El-Hayek et al., 2018a) (Fig. 4A). GOCs obtained from mid-growth stage follicles of *ER-Cre; mTmG* mice
209 carrying the appropriate *Smad4* alleles were exposed to tamoxifen for one day and then incubated for an
210 additional four days. The granulosa cells were then separated from the oocyte and combined with an
211 oocyte that did not carry the *mTmG* gene. These reaggregated GOCs were incubated for an additional 6
212 days, then fixed and stained using anti-GFP (Fig. 4B).

213 When the entire population of granulosa cells in the reaggregated GOCs was analyzed, there was a ~30%
214 reduction in mean volume in the *Smad4*$^{fl/fl}$ cells as compared to *Smad4*$^{+/+}$ cells (394.5 +/- 18.8 vs 279.8 +/-
215 16.6; n=185, 159; $p<0.0001$) and no difference in cell sphericity (Fig. 4C), as observed using intact GOCs.

216 There was no difference between genotypes, however, in mean volume among the cells whose TZPs were
217 characterized (Fig. 4D). Within this group, the mean number of TZPs per cell was reduced by ~50%, from
218 14.2 +/- 2.0 (n=16) in the *Smad4*$^{+/+}$ cells to 6.84 +/- 1.1 (n=25) in the *Smad4*$^{fl/fl}$ cells (Fig. 4D, p=0.001). A
219 ~20% increase in the mean length of the TZPs of *Smad4*$^{fl/fl}$ cells (3.71 +/- 0.17 vs 4.40 +/- 0.28; n=174, 154;
220 *p*=0.03) was also detected, as in intact GOCs, but no difference in the mean width (Fig. 4E).

221 The increased mean length of the TZPs of *Smad4*$^{fl/fl}$ cells compared to *Smad4*$^{+/+}$ cells prompted us to
222 analyze the trajectory of individual TZPs. We traced their path from their point of origin to their tip, then
223 measured the distance between the point of origin and the oocyte and subtracted from this the distance
224 between the tip and the oocyte. A large positive difference indicates that the tip of the TZP is relatively
225 close to the oocyte; conversely, a small positive or a negative difference indicates that that tip is relatively
226 far from the oocyte (Fig. 4F). This analysis revealed that the mean difference was 50% greater in the
227 *Smad4*$^{fl/fl}$ cells compared to *Smad4*$^{+/+}$ cells (1.61 +/- 0.16 vs 2.40 +/- 0.21; n=174, 157; *p*=0.003) (Fig. 4G).
228 This indicates that the tips of the TZPs of the *Smad4*$^{fl/fl}$ cells were, on average, closer to the oocyte than
229 those of the *Smad4*$^{+/+}$ cells. We also found that the proportion of TZPs that were oriented away from the
230 oocyte trended towards being greater in the *Smad4*$^{+/+}$ cells, although the difference did not reach
231 statistical significance (Fig. 4G). Taken together, the trajectory analyses provide additional evidence that
232 the TZPs of *Smad4*$^{fl/fl}$ cells differ from those of *Smad4*$^{+/+}$ cells.

233 The observation that TZP-number was modestly reduced when intact GOCs were analyzed, yet markedly
234 reduced when oocytes from which the granulosa cells had been stripped were analyzed, suggested that
235 the attachment between the TZPs and oocyte might be weakened when SMAD4 was depleted. To
236 evaluate this, the amount of N-cadherin, which is the principal cell adhesion molecule that has been
237 identified in granulosa cells, was compared between *Smad4*$^{+/+}$ and *Smad4*$^{fl/fl}$ granulosa cells. Consistent
238 with the previous results (see Fig. 1E), SMAD4 was reduced by 73.5 +/- 0.05% in the *Smad4*$^{fl/fl}$ granulosa

239 cells (Fig. 5A, n=6, $p<0.0001$). Strikingly, N-cadherin was reduced by 52.7 +/- 0.04 % (n = 6, $p=0.0004$) in
240 the *Smad4*$^{fl/fl}$ granulosa cells (Fig. 5A). Moreover, Notch2, a transmembrane receptor expressed in
241 granulosa cells that associates with membrane-bound Jagged1 expressed on the oocyte, was reduced by
242 52.6 +/- 0.05% (n=5; $p=0.0003$) in these cells (Fig. 5B). In contrast to the protein, however, there was no
243 detectable reduction in the amount of encoding mRNA in either case as assayed using qRT-PCR, although
244 *Smad4* was reduced in the same samples (Fig. 5C). Thus, a reduction in SMAD4 in granulosa cells is
245 associated with a reduction in certain transmembrane proteins, including those responsible for cell
246 adhesion.

247 As we previously reported that depletion of GDF9, which is secreted by the oocyte and signals in the
248 granulosa cells through SMAD4, was associated with a reduction in mRNAs encoding structural
249 components of TZPs – *Myo10*, *Fscn1*, and *Daam1* (El-Hayek et al., 2018a), we measured the quantity of
250 these mRNAs using qRT-PCR. We found that they were not depleted in the *Smad4*$^{fl/fl}$ granulosa cells
251 compared to the *Smad4*$^{+/+}$ cells (Fig. 5D). This implies either that the SMAD4 which remained was
252 sufficient to induce expression of these genes or the GDF9 regulates their expression through a SMAD4-
253 independent pathway.

254 **Discussion**

255 We have examined the role of SMAD4 establishing the TZPs that connect the granulosa cells to the oocyte.
256 Using a tamoxifen-inducible Cre recombinase strategy, we were able to reduce SMAD4 in the granulosa
257 cells to about 30% of its wild-type level. This reduction was associated with a decrease ranging from 20-
258 50% in the number of TZPs in the granulosa cells assessed as a population (i) in intact GOCs and (ii) after
259 removal of the granulosa cell bodies to increase optical resolution, and as individual cells (iii) in intact
260 GOCs and (iv) in reconstructed complexes. Previous studies where SMAD4, or both SMAD2 and SMAD3,
261 was depleted from granulosa cells described a loose or loss association of the cumulus cells with the

262 oocyte in some follicles (Pangas et al., 2006, Li et al., 2008). Moreover, as described in the Introduction,
263 blocking production of GDF9 by the oocyte leads to a decrease in the number of TZPs (Carabatsos et al.,
264 1998, El-Hayek et al., 2018a). Together these observations suggest that SMAD4 regulates the size of the
265 population of TZPs in growing follicles.

266 The population of TZPs presumably reflects the net result of the generation of new TZPs and the retraction
267 of existing TZPs, as is the case for filopodia (Gallop, 2020, Heckman and Plummer, 2013, Mattila and
268 Lappalainen, 2008). SMAD4 could thus promote either or both processes. The observation that GFP-
269 expressing granulosa cells in reaggregated complexes generated new TZPs implies that SMAD4 is not
270 required for this process, although it does not rule out a role in increasing the rate of generation. A clue
271 to the function of SMAD4 may lie in the observation that the decrease in the number of TZPs in SMAD4-
272 depleted cells was quantitatively greater when the granulosa cell bodies were removed prior to analysis.
273 This suggests that the process of removing the cell bodies also removed the TZPs more easily in the
274 SMAD4-depleted cells than in wild-type cells.

275 In this context, it is intriguing that N-cadherin, which is thought to stabilize attachment of the TZP tips to
276 the oocyte surface, was depleted in the mutant cells. We propose that, by increasing the quantity of N-
277 cadherin in the granulosa cells, SMAD4 increases the strength of adhesion of the TZPs to the oocyte
278 surface (Fig. 6). This in turn would decrease the probability of retraction, thereby increasing the steady-
279 state number of TZPs. This model is consistent with the observation that the non-attached (free-ended)
280 TZPs of SMAD4-depleted cells were on average longer and closer to the oocyte than those of wild-type
281 cells. Specifically, if the ability of the TZPs to establish a stable contact with the oocyte were impaired in
282 SMAD4-depleted cells, a relatively large proportion might continue to 'search' for an attachment and to
283 lengthen during the searching process.

284 Mechanistically, some reports have linked SMAD4 to transcription of the *Cdh2*, which encodes N-cadherin
285 (Kang et al., 2014, Yang et al., 2015), but we did not detect a difference in mRNA quantity between normal
286 and SMAD4-depleted granulosa cells. In view of the reduced quantity in the latter of Notch2, also a
287 membrane-associated protein, it may be speculated that SMAD4 might act more broadly to regulate the
288 expression of genes whose products maintain the normal configuration of the granulosa cell plasma
289 membrane. An alternative explanation is raised by observations that granulosa-cell depletion of SMAD4
290 is associated with the presence of follicles containing luteinized granulosa cells enclosing an entrapped
291 oocyte and increased expression of markers of luteinization, including *Cyp11a1*, *Sfrp4*, *Star* and *Ptgfr*
292 (Pangas et al., 2006). This suggests that the SMAD4-depleted granulosa cells in the GOCs studied here
293 might have become luteinized, and that luteinization in turn caused a reduction in the number of TZPs.
294 We did not detect increased expression of the luteinization markers (unpublished data), suggesting that
295 luteinization did not occur under the conditions of our experiments. This difference may arise because we
296 examined GOCs that had been maintained in vitro, whereas the previous study examined follicles in intact
297 ovaries of prepuberal mice following injection of an FSH analogue.

298 Regardless of the mechanism linking SMAD4 to TZP number, it is noteworthy that the number of TZPs that
299 project from an individual granulosa cells – about 15 in this study and about 40 in a previous study where
300 more advanced (antral) follicles were examined (Baena and Terasaki, 2019) – considerably exceeds the
301 number of filopodia that are present on individual blastomeres of mouse embryos (5-6) (Fierro-Gonzalez
302 et al., 2013) or on chick embryonic cells (~4) (Sagar et al., 2015). SMAD4 may therefore act in granulosa
303 cells to amplify an innate ability to generate filopodia, which become TZPs and increase the efficiency of
304 communication between the growing germ cell and its somatic microenvironment.

305

306

307

308

309 **Methods**

Key Resources Table				
Reagent type	**Designation**	**Source or reference**	**Identifiers**	**Additional information**
gene (mouse)	Smad4	GenBank	Gene ID: 17128	
Strain (mouse)	*Smad4*$^{tm2.1Cxd}$/J	Jackson Laboratories	strain 017462	Supplied by Dr. Daniel. J. Bernard, McGill University
Strain (mouse)	*Amhr2*$^{tm3(cre)Bhr}$	MMRRC	strain 014245-UNC	Supplied by Dr. Makoto Nagano, McGill University
Strain (mouse)	B6.129-*Gt(ROSA)26Sor*$^{tm1(cre/ERT2)Tyj}$/J	Jackson Laboratories	strain 008463	
Strain (mouse)	B6.129(Cg)-*Gt(ROSA)26Sor*$^{tm4(ACTB-tdTomato,-EGFP)Luo}$/J	Jackson Laboratories	strain 007676	
RNA in situ hybridization probe	*Smad4*, exon 8	Advanced Cell Diagnostics	857571	
RNA in situ hybridization probe	*Bacillus subtilis DapB*	Advanced Cell Diagnostics	310043	
Primary antibody	SMAD2/3	Cell Signaling Technology	8685	

Primary antibody	SMAD4	Sigma	HPA019154	
Primary antibody	N-cad	BD Biosciences	B610920	
Primary antibody	Notch	Abcam	Ab8926	
Primary antibody	GFP	Invitrogen	A11122	
Secondary antibody	Goat anti-rabbit IgG-HRP	Promega	W4011	
Secondary antibody	Goat anti-mouse IgG-HRP	Promega	W4021	
Secondary antibody	Donkey anti-rabbit IgG- Alexa 488	Invitrogen	A21206	
Reagent	Tamoxifen	Sigma	T176	
Reagent	Phalloidin	Thermo Fisher	A12380	
Reagent	EdU	Thermo Fisher	C10337	

310

Primers				
Target	**application**	**5-prime**	**3-prime**	**Predicted size**
Smad4 -wt	Genotype	GGGCAGCGTAGCATATAAGA	GACCCAAACGTCACCTTCAG	390
Smad4 - flox	Genotype	GGGCAGCGTAGCATATAAGA	GACCCAAACGTCACCTTCAG	450
Smad4 - recombined	Genotype	TAAGAGCCACAGGGTCAAGC	GACCCAAACGTCACCTTCAG	450
Amhr2-Cre	Genotype	CTCTGGTGTAGCTGATGATC	TAATCGCCATCTTCCAGCAG	380
ER-Cre	Genotype	CGTGATCTGCAACTCAGTC	AGGCAAATTTTGGTGTACGG	150

Smad4	mRNA	TCACAATGAGCTTGCATTCC	CCATCCACAGTCACAACAGG	143
Cdh2 (N-Cad)	mRNA	CCAGGAAAAGTGGCAGGTAG	CACTGTGCTTGGCAAGTTGT	121
Notch2	mRNA	GACCCTATCCTACCCTCTAGTG	AGCAGGATGAAGAACAGGATG	103
Myo10	mRNA	TCCAGACAGACTATGGGCAGG	GGAAGCCATGTCGTCCACG	109
Fscn1	mRNA	AGAACGCCAGCTGCTACTTT	CGAGGAATCACTACCCACCG	331
Daam1	mRNA	GCGGCTGCTCAGAGTATAGAAA	AAACATGGCTTCCCTGTGTTTG	273
RPL-19	mRNA	GAAATCGCCAATGCCAACTC	CTTCCCTATGCCCATATGCC	147

311

312 ***Mouse strains***

313 All experiments were performed in compliance with the regulations and policies of the Canadian Council
314 on Animal Care and were approved by the Animal Care Committee of the Research Institute of the McGill
315 University Health Centre (RI-MUHC, protocol 7783). CD-1 mice were obtained from Charles River (St-
316 Constant, QC). The following transgenic strains were obtained from commercial suppliers: B6.129-
317 *Gt(ROSA)26Sor*$^{tm1(cre/ERT2)Tyj}$/J (hereafter *ER-Cre*) carrying a tamoxifen-inducible sequence encoding Cre
318 recombinase under the control of the promoter of the estrogen receptor 2 gene (Jackson Laboratories,
319 Bar Harbor, ME, strain 008463); B6.129(Cg)-*Gt(ROSA)26Sor*$^{tm4(ACTB-tdTomato,-EGFP)Luo}$/J (Jackson, strain 007676;
320 hereafter *mTmG*) carrying sequences encoding a membrane-targeted tdTomato and membrane-targeted
321 EGFP; Cre-mediated recombination of *loxP* sites switches expression from RFP to EGFP. *Smad4*$^{tm2.1Cxd}$/J
322 (hereafter *Smad4*^{fl}) carrying *loxP* sites flanking exon 8 (Jackson, strain 017462) was kindly supplied by Dr.
323 Daniel Bernard (McGill University). *Amhr2*$^{tm3(cre)Bhr}$ (hereafter *Amhr2-Cre*) carrying a sequence encoding
324 Cre recombinase under the control of the promoter of the Anti-Mullerian hormone receptor 2 gene was
325 kindly supplied by Dr. Makoto Nagano (McGill University).

326 To generate *Amhr2-Cre*$^{+}$*; Smad4*$^{fl/fl}$ females carrying an *mTmG* allele, *Smad4*$^{fl/wt}$; *mTmG*$^{+/+}$ females were
327 crossed with *Amhr2-Cre*$^{+}$*; Smad4*$^{fl/wt}$ males. To generate *ER-Cre*$^{+}$*; Smad4*$^{fl/fl}$ females carrying an *mTmG*

328 allele, *Smad4*$^{fl/wt}$; *mTmG*$^{+/+}$ females were crossed with *ER-Cre*$^{+}$; *Smad4*$^{fl/wt}$ males. *ER-Cre*$^{-}$; *mTmG*$^{+}$;
329 *Smad4*$^{fl/fl}$ females and *ER-Cre*$^{+}$; *mTmG*$^{+}$; *Smad4*$^{wt/wt}$ females served as controls. Genotyping of the offspring
330 was done using the EZ Tissue/Tail DNA Isolation Plus PCR kit (EZ Bioresearch). After DNA extraction from
331 tail snips, PCR was used to detect wild type, floxed and recombined *Smad4* and the presence of *ER-Cre*
332 and *Amhr2-Cre* alleles. Primer sequences are given in Supplemental Table 1.

333 **Tissue embedding and immunohistochemistry**

334 Sections of paraffin-embedded ovaries were deparaffinized using xylene, rehydrated in a decreasing
335 ethanol series (100, 90, 70%) for 3 min each, and then placed in Milli-Q water for 5 min. Slides were heated
336 intermittently in a microwave during 20 min in 0.1 M citrate buffer solution at pH 6.0, washed in PBS for
337 10 min, and blocked with CAS universal blocking solution (Thermo Fisher, 008120) for 30 min at room
338 temperature to reduce nonspecific binding. After overnight incubation with primary antibody, slides were
339 washed three times in PBS at room temperature and then incubated for 1 h at room temperature with
340 secondary antibody with DAPI. Slides were washed twice in PBS for 5 min and mounted on a drop of
341 VECTASHIELD solution (Vector Laboratories, H-1200-10). Images were acquired using a Zeiss LSM 880
342 confocal microscope.

343 **Collection, culture and tamoxifen treatment of granulosa cell-oocyte complexes (GOCs)**

344 GOCs were obtained as previously described (El-Hayek et al., 2018b, O'Brien et al., 2003). Briefly, ovaries
345 of 10- to 12-day-old mice were dissected from the ovarian bursa. Follicles were mechanically isolated by
346 carefully tearing the ovaries apart and using fine needles to separate the follicles from each other in
347 HEPES-buffered minimal essential medium (MEM, pH 7.2, Life Technologies, Burlington, ON) (MEM-H). A
348 Pipetman P1000 was used to carefully pick up and transfer the individual follicles to dishes containing
349 fresh medium. GOCs were obtained by incubating follicles in the presence of collagenase (10 µg/ml;

350 Cedarlane, Burlington, ON) and DNase I (10 µg/ml; Sigma) for 5 min at 37°C in air. GOCs were collected
351 and briefly washed in $NaHCO_3$-buffered MEM (MEM-C) and cultured in 4-well plates containing 500 µl of
352 MEM-C supplemented with ITS (10 µg/mL insulin, 5.5 µg/mL transferrin and 5 ng/mL selenium; Sigma),
353 FSH (10 mIU/ml; EMD Serono, Mississauga, ON), and estradiol (10 nM, Sigma, E2758) in an atmosphere
354 of 5% CO_2 in air. To induce Cre-mediated recombination of the *Smad4* allele, GOCs were incubated with
355 4-hydroxytamoxifen (1 µg/ml, Sigma, T176) in the above medium for 24 hours. They were then transferred
356 to medium without tamoxifen.

357 **Immunoblotting**

358 Cell samples were lysed in 10 µl of Laemmli buffer. After denaturation at 95◦C for 10 min, proteins were
359 separated using 4–15% precast polyacrylamide gels (BioRad, 4568085) and transferred onto a
360 polyvinylidene fluoride membrane (Amersham, Oakville, ON, Canada) under constant voltage. The
361 membrane was subsequently blocked using 5% BSA, in 0.1% Tween-PBS. The membrane was washed
362 three times in Tween-PBS and incubated with primary antibody overnight at 4◦C. After washing for 45
363 min, the membrane was incubated in secondary antibody conjugated to horseradish peroxidase
364 (Promega) at a dilution of 1:5000 for 1h at room temperature. After washing for 30 min, bound antibody
365 was revealed using ECL+ (Amersham).

366 **RNA purification and quantitative real-time PCR**

367 RNA was extracted using a Picopure RNA isolation kit (Life Technologies) following the manufacturer's
368 instructions and eluted in 10 µL of the provided elution buffer, as described (El-Hayek *et al*, 2018a). Briefly,
369 SuperScript II Reverse Transcription kit (Life Technologies) was used to generate cDNA. PCR amplification
370 was performed using a Corbett Rotorgene 6000 (Montreal Biotech, Montreal, QC). Each reaction
371 contained 4 µL of EvaGreen Mix (Montreal Biotech), 13 µL of UltraPure DNase/RNase-free distilled water

372 (Life Technologies), 1 µL of 10 mM primers and 2 µL of cDNA (diluted 1:20 from original stock). Primers
373 were designed using Primer-BLAST (National Institutes of Health) and obtained from Sigma. For each
374 primer pair, a standard curve was generated using serial dilutions of cDNA prepared from ovarian RNA
375 and used to determine the efficiency of amplification. Melt-curve analysis and electrophoresis of
376 amplified products confirmed that only a single product of the expected size was generated. Data was
377 analyzed using software provided by the manufacturer. Relative quantities of amplified product were
378 calculated according to 2-ΔΔCT method, using *Rpl19* for normalization.

379 **Immunofluorescence**

380 GOCs and denuded oocytes were fixed for 15 min in freshly prepared 2% (w/v) para-formaldehyde (Fisher
381 Scientific 04042) in PBS (pH 7.2) containing 0.1% Triton X-100 (ACROS 9002-93-1) (PBST), then washed in
382 PBST. The specimens were incubated overnight in primary antibody in PBST at 4 °C with gentle agitation,
383 washed twice in PBST, then incubated for 1 h at room temperature in the secondary antibody as well as
384 phalloidin and DAPI in PBST, then washed in PBST. GOCs or denuded oocytes were placed in a 2 µl drop
385 of PBS containing 0.3% polyvinylpyrrolidone (Sigma, PVP360) on a glass bottom dish covered with mineral
386 oil. Images were acquired using a Zeiss LSM880 confocal microscope. Images were obtained as 16-bit RGB
387 stack files. GOCs were imaged with a Plan Apo 63x/1.4 oil immersion objective and the following lasers
388 and filters (in parentheses): 488 nm (491–553 nm), 561 nm (571–642) and 405 nm (410–484). Laser
389 strength ranged between 1.5 and 2% and digital gain was adjusted until the first saturated pixels were
390 observed for each channel.

391 **EdU incorporation and detection**

392 EdU (5-ethynyl-2'-deoxyuridine) detection was performed on GOCs according to the Click-iT EdU Alexa
393 Fluor 488 Imaging Kit manufacturer's instructions (Molecular Probes, C10337). Briefly, cells were

394 incubated in MEM containing 100 µM EdU for 5 hrs to allow for incorporation into newly synthesized DNA,
395 then fixed, permeabilized, and incubated in Click-iT cocktail reaction for 30 minutes. EdU labeling was
396 visualized by confocal microscopy and quantified with ImageJ (NIH).

397 **In situ hybridization**

398 GOCs were fixed in freshly prepared 2% paraformaldehyde in phosphate-buffered saline (PBS, pH 7) for
399 15 min at room temperature, dehydrated by passing through a gradient of ice-cold methanol (50%, 75%,
400 100%) for 3 minutes each, then sealed and stored at 4°. The next day, the GOCs were rehydrated using
401 the reverse methanol gradient (75%, 50%, PBS) for 3 minutes each. Up to 10 GOCs were placed in the
402 middle of a glass microscope slide, encircled by a hydrophobic barrier created using an Immedge pen, and
403 incubated with protease solution (ACD, 322337) for 20 min. Slides were rinsed 3 times with PBS and
404 processed as indicated by the manufacturer for the BaseScope Assay (Advanced Cell Diagnostics (ACD),
405 323971). Briefly, slides were incubated with the *Smad4* probe specific for the exon8 allele (ACD, 857571)
406 or negative control probe against *Bacillus subtilis DapB* (ACD, 310043) at 40◦C for 2 h in a HybEZ oven.
407 Subsequent amplification and detection steps were performed as recommended by the manufacturer and
408 slides were taken for image acquisition using a Zeiss LSM 880 confocal microscope.

409 **Fluorescence-activated cell sorting**

410 GOCs were dissected from the ovaries of 12-15 d-old *Amhr2-Cre*$^{+}$*; mTmG*$^{+}$*; Smad4*$^{fl/fl}$ mice or were
411 collected after tamoxifen treatment and culture in the case of *ER-Cre+; mTmG+ Smad4*$^{fl/fl}$ mice. GOCs
412 were dissected from *Amhr2-Cre*$^{-}$ and *ER-Cre-* littermates were used as negative controls of EGFP
413 expression**.** They were transferred to a 4-well dish containing Ca-free MEM (Thermo Fisher, 21068028)
414 supplement with 0.25% trypsin (Thermo Fisher, 25200056), 1mM EDTA (Sigma) and DNAse I for several
415 minutes. After pipetting up and down for a few times to dissociate the cells, fetal bovine serum was added

416 (4% final concentration) to inactivate the trypsin. Cells were centrifuged at 1500xg for 5 minutes and
417 supernatant was carefully removed under the dissecting microscope to better visualise the pellet. FACs
418 buffer containing PBS, 1%FBS, 1mM EDTA and 1mg/ml of DAPI was used to resuspend the pellet. Cells
419 were resuspended and passed through a Flowmi® 40-µm strainer (Merck,BAH136800040) to remove
420 oocytes and cell clumps, and then kept on ice for sorting. Resulting granulosa cells were analyzed on a BD
421 FACSAria Fusion 8.0.2 sorter at the Immunophenotyping Facility of the RI-MUHC. All events were collected
422 for each sample. A 488-nm excitation laser was used for both Tomato and EGFP excitation since the
423 wavelength of 488 nm falls within the peak excitation of EGFP but only at 25% of peak excitation for
424 tdTomato. Data were analyzed using FlowJo FACS analysis software. Cells were gated for singlets (using
425 forward scatter vs. side scatter area), viability (DAPI scatter vs. side scatter area)], and fluorescence (FITC
426 and PE) without compensation.

427 **Measurement of granulosa cell-oocyte communication using fluorescence recovery after**
428 **photobleaching (FRAP)**

429 A protocol for FRAP was adapted from our previous study (El-Hayek & Clarke, 2015). GOCs were incubated
430 for 15 min in MEM supplemented with calcein-AM and then for 60 min in calcein-free MEM to allow
431 transfer of calcein from the granulosa cells into oocyte. A circular region of interest of fixed diameter (10
432 µm, to ensure the bleaching did not extend to the surrounding granulosa cells) was set in the center of
433 the enclosed oocyte and subjected to 60 repetitive bleaches of 50 iterations (1 min total duration) using
434 the argon laser at 50% transmission strength. The intensity of fluorescence in the oocyte and the layer of
435 granulosa cells immediately surrounding it was recorded before bleaching and after the 10th, 20th, 30th,
436 40th, 50th, and 60th bleaching. Fluorescence was calculated as intensity of fluorescence in granulosa cell
437 layer at each time point divided by the pre-bleach intensity of the layer. As oocytes of all experimental
438 groups were subjected to the same bleaching procedure within the fixed ROI, the loss in fluorescence was

439 further divided by initial pre-bleach intensity of the oocyte normalized to intensity of fluorescence in
440 oocyte at the given time point, in order to correct for differences in bleaching effect in oocytes of different
441 sizes.

442 **Generation of granulosa cell-oocyte reaggregates**

443 GOCs were obtained from 12-day *ER/Cre*$^{+}$*; mTmG*$^{+}$*; Smad4*$^{+/+}$ and *ER-Cre*$^{+}$*; mTmG*$^{+}$*; Smad4*$^{fl/fl}$ mice,
444 exposed to tamoxifen for 24 hr and incubated for an additional five days as described above. They were
445 then incubated in Ca-Mg-free PBS and drawn in and out of a mouth-controlled micropipette to generate
446 a suspension of denuded oocytes surrounded by the zona pellucida and individual or small clumps of
447 granulosa cells. Briefly, the granulosa cells were deposited together with oocytes from CD-1 mice into the
448 base of a 200-µl microfuge tube and PBS was added to a total volume of 100 µl. The tube was spun at top
449 speed in a microcentrifuge for one minute, then rotated 180° and centrifuged for one minute. This step
450 was repeated twice more. The tube was then cut near the base and the cell-pellet was carefully scooped
451 out and incubated for 2 days in 4-well plates in MEM supplemented with FSH, estradiol and ITS. At the
452 end of the incubation period, complexes of oocytes surrounded by granulosa cells were fixed and
453 processed for analysis.

454 **Image analysis**

455 To quantify the number of F-actin-stained-TZPs, a confocal optical section was obtained at the equatorial
456 plane of the oocyte. Using Fiji software (National Institutes of Health, Bethesda, MD), a segmented circle
457 was drawn around the oocyte in the middle of the zona pellucida, and the fluorescence intensity at each
458 point on the line was obtained. Each point whose value was above the background value of the oocyte
459 cytoplasm and higher than each of its immediately neighboring points was counted as a TZP.

460 To quantify EdU incorporation in granulosa cells, Fiji was used to calculate the ratio of Edu-labelled cells
461 per GOC by dividing the number of EdU-positive cells by the total number of cells counterstained with
462 DAPI.

463 To individually segment granulosa cells and their corresponding TZPs, Imaris 9.7.2 Software (Bitplane) was
464 used. First, z-stacks of 0.2 µm thickness covering the middle region of a follicle were imaged to obtain a
465 conventional 2D Maximum Intensity Projection (MIP). Then, a 3D rendered segmentation of GFP-positive
466 granulosa cells was created with the "Cell detection" tool where cell boundaries were detected based on
467 GFP membrane staining. Smallest diameter was set to 100µm, membrane detail of 0.2 µm and the
468 threshold was adjusted based on local contrast. Segmented cells with a volume less than 100µm^2 were
469 deleted and fusing or fragmented cells were edited using the "merge" or "split" tools to match the original
470 image. The oocyte was also segmented using the phalloidin red channel. After edition, cells were
471 converted to surface objects with the tool "Convert to surfaces" to record their measurements. To render
472 individual TZPs, the "Filament tracer" tool and semi-automated tracing with the tool "Autopath" was used
473 to draw the path of each TZP from the granulosa cell body (start) to the oocyte surface (end)
474 (Supplemental Figure 1A). TZP diameter (thickness) was calculated automatically with a minimum
475 diameter of 0.1 µm. To determine the distance of the TZP tip to the oocyte surface, the segmented TZP
476 was automatically divided into discrete spots using the extension "Filament to Spots". This allowed the
477 calculation of the distance from each spot to the oocyte surface. All measurements were exported using
478 the "distance to oocyte surface" from each TZP spot. To determine the TZP orientation (away or towards
479 the oocyte), the distance of the spot located at the TZP start was subtracted from the distance of the spot
480 located at the TZP tip. A positive difference indicates that the TZP tip is closer to the oocyte and a negative
481 difference indicates that the TZP tip is farther from the oocyte (Supplemental Figure 1B).

482 **Statistical analysis**

483 Data are presented as mean ± standard error of mean and were analyzed and represented using GraphPad
484 Prism 8.4.2 software. Statistical significance was evaluated using one- or two-sample two-tailed t-tests.

485 **Acknowledgements**

486 We thank Drs. Shibo Feng and Min Fun (RI-MUHC Imaging Platform) and Marie-Hélène Lacombe, Hélène
487 Pagé-Veillette and Dr. Ekaterina Iourtchenko (RI-MUHC Immunophenotyping Platform) for their
488 invaluable assistance. We acknowledge the core facility CELLIM supported by MEYS CR (LM2023050
489 Czech-BioImaging) for their generous support and assistance in obtaining image analysis data using Imaris,
490 and thank our colleagues for advice and discussion. Supported by grants to H.J.C. from the Canadian
491 Institutes of Health Research and the Natural Sciences and Engineering Research Council. H.J.C. gratefully
492 acknowledges the support of the Richard Cruess Chair in Reproductive Biology at McGill University.

493 **Author contributions**

494 Conceptualization: S.G.A. and H.C.

495 Methodology: S.G.A., Q.Y. and H.C.

496 Investigation: S.G.A. and Q.Y.

497 Funding acquisition: H.C.

498 Supervision: S.G.A. and H.C.

499 Writing – original draft: S.G.A. and H.C.

500 Writing – review and editing: All authors have read and agreed to the final version of the manuscript.

501 **Conflict of interest**

502 The authors declare no conflicts of interest.

503 **References**

504 AASHAQ, S., BATOOL, A., MIR, S. A., BEIGH, M. A., ANDRABI, K. I. & SHAH, Z. A. 2022. TGF-β signaling: A
505 recap of SMAD-independent and SMAD-dependent pathways. *Journal of Cellular Physiology,*
506 237**,** 59-85.
507 ALBERTINI, D. F. & RIDER, V. 1994. Patterns of intercellular connectivity in the mammalian cumulus-
508 oocyte complex. *Microsc Res Techn,* 27**,** 125-133.
509 ARAGÓN, E., WANG, Q., ZOU, Y., MORGANI, S. M., RUIZ, L., KACZMARSKA, Z., SU, J., TORNER, C., TIAN, L.,
510 HU, J., SHU, W., AGRAWAL, S., GOMES, T., MÁRQUEZ, J. A., HADJANTONAKIS, A. K., MACIAS, M.
511 J. & MASSAGUÉ, J. 2019. Structural basis for distinct roles of SMAD2 and SMAD3 in FOXH1
512 pioneer-directed TGF-β signaling. *Genes Dev,* 33**,** 1506-1524.
513 BAENA, V. & TERASAKI, M. 2019. Three-dimensional organization of transzonal projections and other
514 cytoplasmic extensions in the mouse ovarian follicle. *Sci Rep,* 9**,** 1262.
515 CARABATSOS, M. J., ELVIN, J., MATZUK, M. M. & ALBERTINI, D. F. 1998. Characterization of oocyte and
516 follicle development in growth differentiation factor-9-deficient mice. *Dev Biol,* 204**,** 373-384.
517 CARABATSOS, M. J., SELLITTO, C., GOODENOUGH, D. A. & ALBERTINI, D. F. 2000. Oocyte-granulosa cell
518 heterologous gap junctions are required for the coordination of nuclear and cytoplasmic meiotic
519 competence. *Dev Biol,* 226**,** 167-179.
520 CLARKE, H. J. 2018. Regulation of germ cell development by intercellular signaling in the mammalian
521 ovarian follicle. *Wiley Interdiscip Rev Dev Biol,* 7**,** 10.1002/wdev.294.
522 CLARKE, H. J. 2022. Transzonal projections: Essential structures mediating intercellular communication
523 in the mammalian ovarian follicle. *Mol Reprod Dev,* 89**,** 509-525.
524 CROZET, F., LETORT, G., BULTEAU, R., DA SILVA, C., EICHMULLER, A., TORTORELLI, A. F., BLÉVINAL, J.,
525 BELLE, M., DUMONT, J., PIOLOT, T., DAUPHIN, A., COULPIER, F., CHÉDOTAL, A., MAÎTRE, J. L.,
526 VERLHAC, M. H., CLARKE, H. J. & TERRET, M. E. 2023. Filopodia-like protrusions of adjacent
527 somatic cells shape the developmental potential of oocytes. *Life Sci Alliance,* 6**,** e202301963.
528 DERYNCK, R. & BUDI, E. H. 2019. Specificity, versatility, and control of TGF-β family signaling. *Sci Signal,*
529 12**,** eaav5183.
530 DOHERTY, C. A., AMARGANT, F., SHVARTSMAN, S. Y., DUNCAN, F. E. & GAVIS, E. R. 2022. Bidirectional
531 communication in oogenesis: a dynamic conversation in mice and Drosophila. *Trends Cell Biol,*
532 32**,** 311-323.
533 DONG, J., ALBERTINI, D. F., NISHIMORI, K., KUMAR, R. M., LU, N. & MATZUK, M. 1996. Growth
534 differentiation factor-9 is required during early ovarian folliculogenesis. *Nature,* 383**,** 531-535.
535 DRAGOVIC, R. A., RITTER, L. J., SCHULZ, S. J., AMATO, F., THOMPSON, J. G., ARMSTRONG, D. T. &
536 GILCHRIST, R. B. 2007. Oocyte-secreted factor activation of SMAD 2/3 signaling enables initiation
537 of mouse cumulus cell expansion. *Biol Reprod,* 76**,** 848-857.
538 EL-HAYEK, S. & CLARKE, H. J. 2016. Control of oocyte growth and development by intercellular
539 communication within the follicular niche. *Res Probl Cell Differ,* 58**,** 191-224.
540 EL-HAYEK, S., YANG, Q., ABBASSI, L., FITZHARRIS, G. & CLARKE, H. J. 2018a. Mammalian oocytes locally
541 remodel follicular architecture to provide the foundation for germline-soma communication.
542 *Current Biology,* 28**,** 1124-1131.
543 EL-HAYEK, S., YANG, Q. & CLARKE, H. J. 2018b. Growth in vitro of granulosa cell-oocyte complexes of the
544 mouse. *Methods Mol Biol,* 1818**,** 1-11.

545 ELVIN, J., YAN, C., WANG, P., NISHIMORI, K. & MATZUK, M. 1999a. Molecular characterization of the
546 follicular defects in the growth differentiation factor 9-deficient ovary. *Mol Endocrinol,* 13**,** 1018-
547 1034.
548 ELVIN, J. A., CLARK, A. T., WANG, P., WOLFMAN, N. M. & MATZUK, M. M. 1999b. Paracrine actions of
549 growth differentiation factor-9 in the mammalian ovary. *Mol Endocrinol,* 13**,** 1035-48.
550 EPPIG, J. J. 1979. A comparison between oocyte growth in coculture with granulosa cells and oocytes
551 with granulosa cell-oocyte junctional contact maintained in vitro. *J Exp Zool,* 209**,** 345-53.
552 FIERRO-GONZALEZ, J. C., WHITE, M. D., SILVA, J. C. & PLACHTA, N. 2013. Cadherin-dependent filopodia
553 control preimplantation embryo compaction. *Nat Cell Biol,* 15**,** 1424-33.
554 GALLOP, J. L. 2020. Filopodia and their links with membrane traffic and cell adhesion. *Semin Cell Dev*
555 *Biol,* 102**,** 81-89.
556 GITTENS, J. E. & KIDDER, G. M. 2005. Differential contributions of connexin37 and connexin43 to
557 oogenesis revealed in chimeric reaggregated mouse ovaries. *J Cell Sci,* 118**,** 5071-8.
558 GUGLIELMI, L., HELIOT, C., KUMAR, S., ALEXANDROV, Y., GORI, I., PAPALEONIDOPOULOU, F.,
559 BARRINGTON, C., EAST, P., ECONOMOU, A. D., FRENCH, P. M. W., MCGINTY, J. & HILL, C. S. 2021.
560 Smad4 controls signaling robustness and morphogenesis by differentially contributing to the
561 Nodal and BMP pathways. *Nature Communications,* 12**,** 6374.
562 HAO, X., YUAN, F., CUI, Y. & ZHANG, M. 2022. Oocyte-secreted factor TGFB2 enables mouse cumulus cell
563 expansion in vitro. *Mol Reprod Dev,* 89**,** 554-562.
564 HECKMAN, C. A. & PLUMMER, H. K., 3RD 2013. Filopodia as sensors. *Cell Signal,* 25**,** 2298-311.
565 HERTA, A.-C., AKIN, N., BILLOOYE, K., SAUCEDO-CUEVAS, L., LOLICATO, F., SEGERS, I., ANCKAERT, E. &
566 SMITZ, J. 2021. Reversing complete mechanical transzonal projections disruption during mouse
567 in vitro follicle culture with unaltered oocyte competence†. *Biology of Reproduction,* 104**,** 1373-
568 1385.
569 JAFFE, L. A. & EGBERT, J. R. 2016. Regulation of mammalian oocyte meiosis by intercellular
570 communication within the ovarian follicle. *Ann Rev Physiol,* 79**,** 237-260.
571 JORGENSEN, J. S. 2013. Defining the neighborhoods that escort the oocyte through its early life events
572 and into a functional follicle. *Mol Reprod Dev,* 80**,** 960-76.
573 JORGEZ, C. J., KLYSIK, M., JAMIN, S. P., BEHRINGER, R. R. & MATZUK, M. M. 2004. Granulosa Cell-Specific
574 Inactivation of Follistatin Causes Female Fertility Defects. *Mol Endocrinol,* 18**,** 953-967.
575 KANG, Y., LING, J., SUZUKI, R., ROIFE, D., CHOPIN-LALY, X., TRUTY, M. J., CHATTERJEE, D., WANG, H.,
576 THOMAS, R. M., KATZ, M. H., CHIAO, P. J. & FLEMING, J. B. 2014. SMAD4 regulates cell motility
577 through transcription of N-cadherin in human pancreatic ductal epithelium. *PLoS One,* 9**,**
578 e107948.
579 KESSEL, R. G., TUNG, H. N., ROBERTS, R. & BEAMS, H. W. 1985. The presence and distribution of gap
580 junctions in the oocyte-follicle cell complex of the zebrafish, Brachydanio rerio. *J Submicrosc*
581 *Cytol,* 17**,** 239-53.
582 LI, Q., PANGAS, S. A., JORGEZ, C. J., GRAFF, J. M., WEINSTEIN, M. & MATZUK, M. M. 2008. Redundant
583 roles of SMAD2 and SMAD3 in ovarian granulosa cells in vivo. *Mol Cell Biol,* 28**,** 7001-7011.
584 LI, R. & ALBERTINI, D. F. 2013. The road to maturation: somatic cell interaction and self-organization of
585 the mammalian oocyte. *Nat Rev Mol Cell Biol,* 14**,** 141-52.
586 LI, Y., SCHANG, G., WANG, Y., ZHOU, X., LEVASSEUR, A., BOYER, A., DENG, C. X., TREIER, M., BOEHM, U.,
587 BOERBOOM, D. & BERNARD, D. J. 2018. Conditional deletion of FOXL2 and SMAD4 in
588 gonadotropes of adult mice causes isolated FSH deficiency. *Endocrinology,* 159**,** 2641-2655.
589 LITSCHER, E. S. & WASSARMAN, P. M. 2020. Zona pellucida proteins, fibrils, and matrix. *Annual Review*
590 *of Biochemistry,* 89**,** 695-715.

591 MACAULAY, A. D., GILBERT, I., CABALLERO, J., BARRETO, R., FOURNIER, E., TOSSOU, P., SIRARD, M. A.,
592 CLARKE, H. J., KHANDJIAN, E. W., RICHARD, F. J., HYTTEL, P. & ROBERT, C. 2014. The gametic
593 synapse: RNA transfer to the bovine oocyte. *Biol Reprod,* 91**,** 90.
594 MARCHAIS, M., GILBERT, I., BASTIEN, A., MACAULAY, A. & ROBERT, C. 2022. Mammalian cumulus-oocyte
595 complex communication: a dialog through long and short distance messaging. *J Assist Reprod*
596 *Genet,* 39**,** 1011-1025.
597 MATTILA, P. K. & LAPPALAINEN, P. 2008. Filopodia: molecular architecture and cellular functions. *Nat*
598 *Rev Mol Cell Biol,* 9**,** 446-54.
599 MCGINNIS, L. K. & KINSEY, W. H. 2015. Role of focal adhesion kinase in oocyte-follicle communication.
600 *Mol Reprod Dev,* 82**,** 90-102.
601 MORA, J. M., FENWICK, M. A., CASTLE, L., BAITHUN, M., RYDER, T. A., MOBBERLEY, M., CARZANIGA, R.,
602 FRANKS, S. & HARDY, K. 2012. Characterization and significance of adhesion and junction-related
603 proteins in mouse ovarian follicles. *Biol Reprod,* 86**,** 153.
604 MOTTA, P., MAKABE, S., NAGURO, T. & CORRER, S. 1994. Oocyte follicle cells association during
605 development of human ovarian follicle. A study by high resolution scanning and transmission
606 electron microscopy. *Arch Histol Cytol,* 57**,** 369 - 394.
607 MOTTERSHEAD, D. G., SUGIMURA, S., AL-MUSAWI, S. L., LI, J. J., RICHANI, D., WHITE, M. A., MARTIN, G.
608 A., TROTTA, A. P., RITTER, L. J., SHI, J., MUELLER, T. D., HARRISON, C. A. & GILCHRIST, R. B. 2015.
609 Cumulin, an oocyte-secreted heterodimer of the transforming growth factor-beta family, is a
610 potent activator of granulosa cells and improves oocyte quality. *J Biol Chem,* 290**,** 24007-24020.
611 NAGAMATSU, G., SHIMAMOTO, S., HAMAZAKI, N., NISHIMURA, Y. & HAYASHI, K. 2019. Mechanical
612 stress accompanied with nuclear rotation is involved in the dormant state of mouse oocytes. *Sci*
613 *Adv,* 5**,** eaav9960.
614 NORRIS, R. P., RATZAN, W. J., FREUDZON, M., MEHLMANN, L. M., KRALL, J., MOVSESIAN, M. A., WANG,
615 H., KE, H., NIKOLAEV, V. O. & JAFFE, L. A. 2009. Cyclic GMP from the surrounding somatic cells
616 regulates cyclic AMP and meiosis in the mouse oocyte. *Development,* 136**,** 1869-1878.
617 O'BRIEN, M. J., PENDOLA, J. K. & EPPIG, J. J. 2003. A revised protocol for in vitro development of mouse
618 oocytes from primordial follicles dramatically improves their developmental competence. *Biol*
619 *Reprod,* 68**,** 1682-1686.
620 PANGAS, S. A., LI, X., ROBERTSON, E. J. & MATZUK, M. M. 2006. Premature luteinization and cumulus
621 cell defects in ovarian-specific Smad4 knockout mice. *Mol Endocrinol,* 20**,** 1406-1422.
622 PANGAS, S. A. & RAJKOVIC, A. 2015. Follicular Development: Mouse, Sheep, and Human Models. *In:*
623 PLANT, T. M. & ZELEZNIK, A. J. (eds.) *Knobil and Neill's Physiology of Reproduction (Fourth*
624 *Edition).* San Diego: Academic Press.
625 PATTON, B. K., MADADI, S. & PANGAS, S. A. 2021. Control of ovarian follicle development by TGFβ family
626 signaling. *Curr Opin Endocr Metab Res,* 18**,** 102-110.
627 PENG, D., FU, M., WANG, M., WEI, Y. & WEI, X. 2022. Targeting TGF-β signal transduction for fibrosis and
628 cancer therapy. *Molecular Cancer,* 21**,** 104.
629 PENG, J., LI, Q., WIGGLESWORTH, K., RANGARAJAN, A., KATTAMURI, C., PETERSON, R. T., EPPIG, J. J.,
630 THOMPSON, T. B. & MATZUK, M. M. 2013. Growth differentiation factor 9:bone morphogenetic
631 protein 15 heterodimers are potent regulators of ovarian functions. *Proc Natl Acad Sci U S A,*
632 110**,** E776-85.
633 RICHANI, D., DUNNING, K. R., THOMPSON, J. G. & GILCHRIST, R. B. 2021. Metabolic co-dependence of
634 the oocyte and cumulus cells: essential role in determining oocyte developmental competence.
635 *Human Reproduction Update,* 27**,** 27-47.
636 ROBERT, C. 2021. Nurturing the egg: the essential connection between cumulus cells and the oocyte.
637 *Reprod Fertil Dev,* 34**,** 149-159.

638 SAATCIOGLU, H. D., CUEVAS, I. & CASTRILLON, D. H. 2016. Control of oocyte reawakening by Kit. *PLoS*
639 *Genet,* 12**,** e1006215.
640 SAGAR, PRÖLS, F., WIEGREFFE, C. & SCAAL, M. 2015. Communication between distant epithelial cells by
641 filopodia-like protrusions during embryonic development. *Development,* 142**,** 665-71.
642 SCHROEDER, T. E. 1981. Microfilament-mediated surface change in starfish oocytes in response to 1-
643 methyladenine: implications for identifying the pathway and receptor sites for maturation-
644 inducing hormones. *J Cell Biol,* 90**,** 362-71.
645 SIMON, A., GOODENOUGH, D., LI, E. & PAUL, D. 1997. Female infertility in mice lacking connexin 37.
646 *Nature,* 385**,** 525-529.
647 WASSARMAN, P. M. & LITSCHER, E. S. 2018. The mouse egg's zona pellucida. *Curr Top Dev Biol,* 130**,** 331-
648 356.
649 WIGGLESWORTH, K., LEE, K. B., O'BRIEN, M. J., PENG, J., MATZUK, M. M. & EPPIG, J. J. 2013.
650 Bidirectional communication between oocytes and ovarian follicular somatic cells is required for
651 meiotic arrest of mammalian oocytes. *Proc Natl Acad Sci U S A,* 110**,** E3723-9.
652 WINTERHAGER, E. & KIDDER, G. M. 2015. Gap junction connexins in female reproductive organs:
653 implications for women's reproductive health. *Hum Reprod Update,* 21**,** 340-52.
654 WU, X., CHEN, L., BROWN, C. A., YAN, C. & MATZUK, M. M. 2004. Interrelationship of growth
655 differentiation factor 9 and inhibin in early folliculogenesis and ovarian tumorigenesis in mice.
656 *Mol Endocrinol,* 18**,** 1509-19.
657 XIE, J., XU, X. & LIU, S. 2023. Intercellular communication in the cumulus–oocyte complex during
658 folliculogenesis: A review. *Frontiers in Cell and Developmental Biology,* 11.
659 YAN, C., WANG, P., DEMAYO, J., DEMAYO, F. J., ELVIN, J. A., CARINO, C., PRASAD, S. V., SKINNER, S. S.,
660 DUNBAR, B. S., DUBE, J. L., CELESTE, A. J. & MATZUK, M. M. 2001. Synergistic roles of bone
661 morphogenetic protein 15 and growth differentiation factor 9 in ovarian function. *Mol*
662 *Endocrinol,* 15**,** 854-66.
663 YANG, H., WANG, L., ZHAO, J., CHEN, Y., LEI, Z., LIU, X., XIA, W., GUO, L. & ZHANG, H. T. 2015. TGF-β-
664 activated SMAD3/4 complex transcriptionally upregulates N-cadherin expression in non-small
665 cell lung cancer. *Lung Cancer,* 87**,** 249-57.
666 YU, C., ZHANG, Y. L. & FAN, H. Y. 2013. Selective Smad4 knockout in ovarian preovulatory follicles results
667 in multiple defects in ovulation. *Mol Endocrinol,* 27**,** 966-78.
668 ZHANG, H., RISAL, S., GORRE, N., BUSAYAVALASA, K., LI, X., SHEN, Y., BOSBACH, B., BRÄNNSTRÖM, M. &
669 LIU, K. 2014. Somatic cells initiate primordial follicle activation and govern the development of
670 dormant oocytes in mice. *Curr Biol,* 24**,** 2501-2508.
671 ZHANG, M., SU, Y. Q., SUGIURA, K., XIA, G. & EPPIG, J. J. 2010. Granulosa cell ligand NPPC and its
672 receptor NPR2 maintain meiotic arrest in mouse oocytes. *Science,* 330**,** 366-9.
673 ZHANG, Y., WANG, Y., FENG, X., ZHANG, S., XU, X., LI, L., NIU, S., BO, Y., WANG, C., LI, Z., XIA, G. &
674 ZHANG, H. 2021. Oocyte-derived microvilli control female fertility by optimizing ovarian follicle
675 selection in mice. *Nat Commun,* 12**,** 2523.

676

677

678 **Figure 1. SMAD4 is efficiently depleted in granulosa cells of GOCs in vitro using tamoxifen-induced Cre**
679 **recombinase**

680 A. Immunoblot of primordial follicles, growing follicles, and granulosa cells and oocytes isolated from
681 antral follicles, probed using anti-SMAD4 and anti-SMAD2/3.
682 B. Breeding scheme to delete *Smad4* in the granulosa cells using *Amhr2-Cre*. The *mTmG* cassette
683 enables Cre recombinase activity to be verified through expression of EGFP.
684 C. Left: Confocal images of histological sections of paraffin-embedded 12-d ovary (i, ii) and an isolated
685 follicle (iii) stained using an anti-GFP antibody and DAPI to counterstain DNA. Relatively few
686 granulosa cells are GFP-positive (arrow in iii). Scale bars: 50 µm, 20 µm, 10 µm. Right: Histogram and
687 chart showing the percentage of FACS-sorted GFP+ and GFP- granulosa cells from growing follicles.
688 Granulosa cells expressing both td tomato and GFP and GFP alone were scored as GFP+.
689 D. Breeding scheme to delete *Smad4* in vitro using generate tamoxifen-inducible *ER-Cre*. The *mTmG*
690 cassette enables Cre recombinase activity to be verified through expression of EGFP.
691 E. Left: Schematic illustrating time-line of GOC exposure to tamoxifen and subsequent incubation.
692 Center: Bright-field image of GOCs following incubation and confocal image of a representative GOC
693 stained using anti-GFP antibody and DAPI to counterstain DNA. Scale bar = 10µm and 100µm,
694 respectively. Right: Bar chart showing the percentage of FACS-sorted GFP+ and GFP- granulosa cells
695 from GOCs. Granulosa cells expressing td tomato and GFP and GFP alone are counted as GFP+.
696 F. Left: Confocal image of representative GOCs stained with single-molecule RNA FISH probe for *Smad4*
697 exon 8 and DAPI to counterstain DNA. Right: Mean and SEM of the average number of *Smad4* mRNA
698 foci per cell (left) and relative mRNA amounts of *Smad4* quantified using qRT-PCR (right) in granulosa
699 cells five days after tamoxifen treatment.
700 G. Immunoblot and plot of mean and SEM of SMAD4 protein content in granulosa cells from GOCs five
701 days after tamoxifen treatment.

Statistical analysis using t-test (F, left) and one-sample t-test (F, right and G), ***P< 0.001; ****P < 0.0001.

705 **Figure 2. Depletion of SMAD4 reduces TZP-number but does not affect granulosa cell communication**
706 **with the oocyte or proliferation.**

707 A. Confocal images of GOCs five days after tamoxifen treatment stained with anti-GFP, phalloidin to
708 visualize F-actin and DAPI to counterstain DNA. Arrow shows GFP-labelled TZPs. Scale bar = 20 µm.

709 B. Mean and SEM of oocyte diameter and TZP number five days after tamoxifen treatment. TZP
710 number in each GOC is normalized to the oocyte diameter.

711 C. Confocal image of a denuded GOC five days after tamoxifen treatment and removal of the
712 granulosa cells, stained with anti-GFP, phalloidin to visualize F-actin and DAPI to counterstain DNA.
713 Arrow shows phalloidin-labelled TZPs that remain embedded in the zona pellucida. Scale bar =
714 20µm.

715 D. Mean and SEM of oocyte diameter and TZP number five days after tamoxifen treatment in denuded
716 GOCs. TZP number for each specimen is normalized to the oocyte diameter.

717 E. Left: Time course of fluorescence recovery in oocyte of GOCs following bleaching. Each line
718 represents an individual GOC. Right: Mean and SEM of the ratio of the final to pre-bleach
719 fluorescence in each GOC.

720 F. Left: Confocal image of a GOC after tamoxifen treatment followed by treatment with EdU and
721 visualization. DNA stained using DAPI. Scale bar = 20 µm. Right: Mean and SEM of the ratio of Edu-
722 labelled cells to the total number of cells.

723 Statistical analysis using t-test, *P< 0.05; ****P < 0.0001; ns, not significant.

724

725 **Figure 3. Depletion of SMAD4 in GOCs reduces the number of TZPs per granulosa cell and alters their**

726 **morphometric parameters.**

727 A. Schematic illustrating the experimental protocol. GFP+ granulosa cells in clusters were used for

728 calculations in C and individual GFP+ granulosa cells were used for calculations in D.

729 B. Three-dimensional reconstruction of a GOC, showing granulosa cell bodies, TZPs and oocyte cortex.

730 Serial optical confocal sections were processed using Imaris software. GOCs were stained using

731 anti-GFP (green), phalloidin (red) and DAPI (blue). Scale bar = 10 µm (upper, middle), 3 µm (lower).

732 C. Mean and SEM of volumes and sphericities of individual granulosa cells from a cluster and those

733 selected for TZP analyses.

734 D. Mean and SEM of volumes of individual granulosa cells selected for TZP analysis, number of TZPs

735 per cell, TZP length and width.

736 Statistical analysis using t-test, ****$P < 0.0001$; ns, non-significant.

737

738 **Figure 4. Depletion of SMAD4 in reaggregates reduces the number of newly generated TZPs and alters**

739 **their morphometric parameters.**

740 A. Schematic illustrating the reaggregation procedure.

741 B. Three-dimensional reconstruction of a reaggregate, showing granulosa cell bodies, TZPs and oocyte

742 cortex. Serial optical confocal sections were processed using Imaris software. GOCs were stained

743 using anti-GFP (green), phalloidin (red) and DAPI (blue). Scale bar =10 µm (upper), 3 µm (lower).

744 C. Mean and SEM of volumes and sphericities of individual granulosa cells.

745 D, E Mean and SEM of volumes of individual granulosa cells, number of TZPs per cell, TZP length and TZP

746 width.

747 F. Upper: Schematic illustrating how the distance from the origin and the tip, respectively, of TZPs

748 (blue) and non-TZP projections (red) to the oocyte surface was determined. Lower: TZP trajectories

749 of 3D-reconstructed TZPs, representing the distance from origin relative to the position on the TZP

750 axis.

751 G. Left: Mean and SEM of the difference between the distance from the origin and the tip of individual

752 TZPs to the oocyte surface. Blue symbols (>0) represent TZPs oriented towards the oocyte; red

753 symbols (<0) represent non-TZPs oriented away from the oocyte. Right: Mean and SEM of the

754 proportion of TZPs in individual cells that were oriented away from the oocyte.

755 Statistical analysis using t-test, *P < 0.05; **P < 0.01; ****P < 0.0001; ns, non-significant.

756

757 **Figure 5. Expression of transmembrane N-cadherin and Notch proteins is reduced in SMAD4-depleted**

758 **granulosa cells.**

759 A. Immunoblot and graph showing mean and SEM of SMAD4 and N-cadherin in granulosa cells.

760 Protein quantities are normalized to amounts in ER-Cre^{-} cells.

761 B. As in A, showing Notch2.

762 C. Mean and SEM of relative mRNA amounts of *Smad4*, *Cdh2* (encoding N-cadherin), and *Notch2* in

763 granulosa cells purified from GOCs five days after tamoxifen treatment. mRNA quantities are

764 normalized to amounts in ER-Cre^{-} cells.

765 D. As in C, showing *Smad4*, *Myo10, Fscn1* and *Daam1*.

766 Statistical analysis using one-sample t-test, ***P < 0.001; ****P < 0.0001; ns non-significant.

767

768 **Figure 6. Model for regulation of the size of the TZP population.**

769 Upper: Dynamics of an individual TZP. When growing TZP contacts the surface of the oocyte, it becomes
770 stably attached if there is sufficient N-cadherin, as in wild-type cells. In SMAD4-depleted cells, there is
771 insufficient N-cadherin to stabilize the attachment. The TZP may continue to elongate but eventually
772 becomes retracted. Lower: Dynamics of the population of TZPs. Owing to increased stability of
773 attachment of individual TZPs to the oocyte surface, the total number of TZPs becomes larger in wild-
774 type cells than in SMAD4-depleted cells.

775

Figure 1

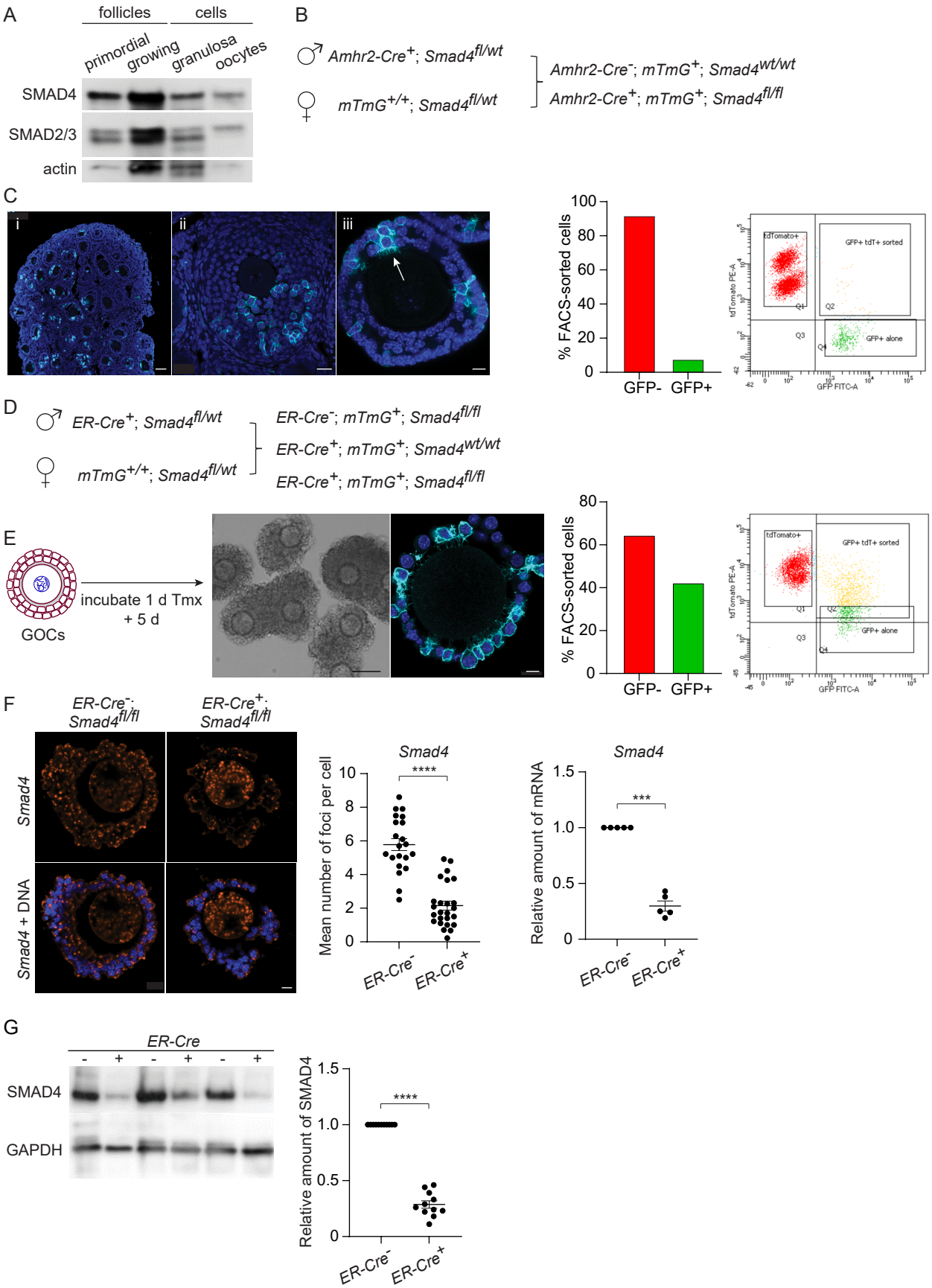
A
follicles
cells
primordial
growing
granulosa
oocytes
SMAD4
SMAD2/3
actin
B
♂ Amhr2-Cre+; Smad4fl/wt
♀ mTmG+/+; Smad4fl/wt
Amhr2-Cre-; mTmG+; Smad4wt/wt
Amhr2-Cre+; mTmG+; Smad4fl/fl
C
i
ii
iii
% FACS-sorted cells
GFP-
GFP+
tdTomato+
GFP+ tdT+ sorted
GFP+ alone
tdTomato PE-A
GFP FITC-A
D
♂ ER-Cre+; Smad4fl/wt
♀ mTmG+/+; Smad4fl/wt
ER-Cre-; mTmG+; Smad4fl/fl
ER-Cre+; mTmG+; Smad4wt/wt
ER-Cre+; mTmG+; Smad4fl/fl
E
GOCs
incubate 1 d Tmx
+ 5 d
% FACS-sorted cells
GFP-
GFP+
F
ER-Cre-; Smad4fl/fl
ER-Cre+; Smad4fl/fl
Smad4
Smad4 + DNA
Smad4
Mean number of foci per cell
****
ER-Cre-
ER-Cre+
Smad4
Relative amount of mRNA
***
ER-Cre-
ER-Cre+
G
ER-Cre
SMAD4
GAPDH
Relative amount of SMAD4
****
ER-Cre-
ER-Cre+

Figure 2

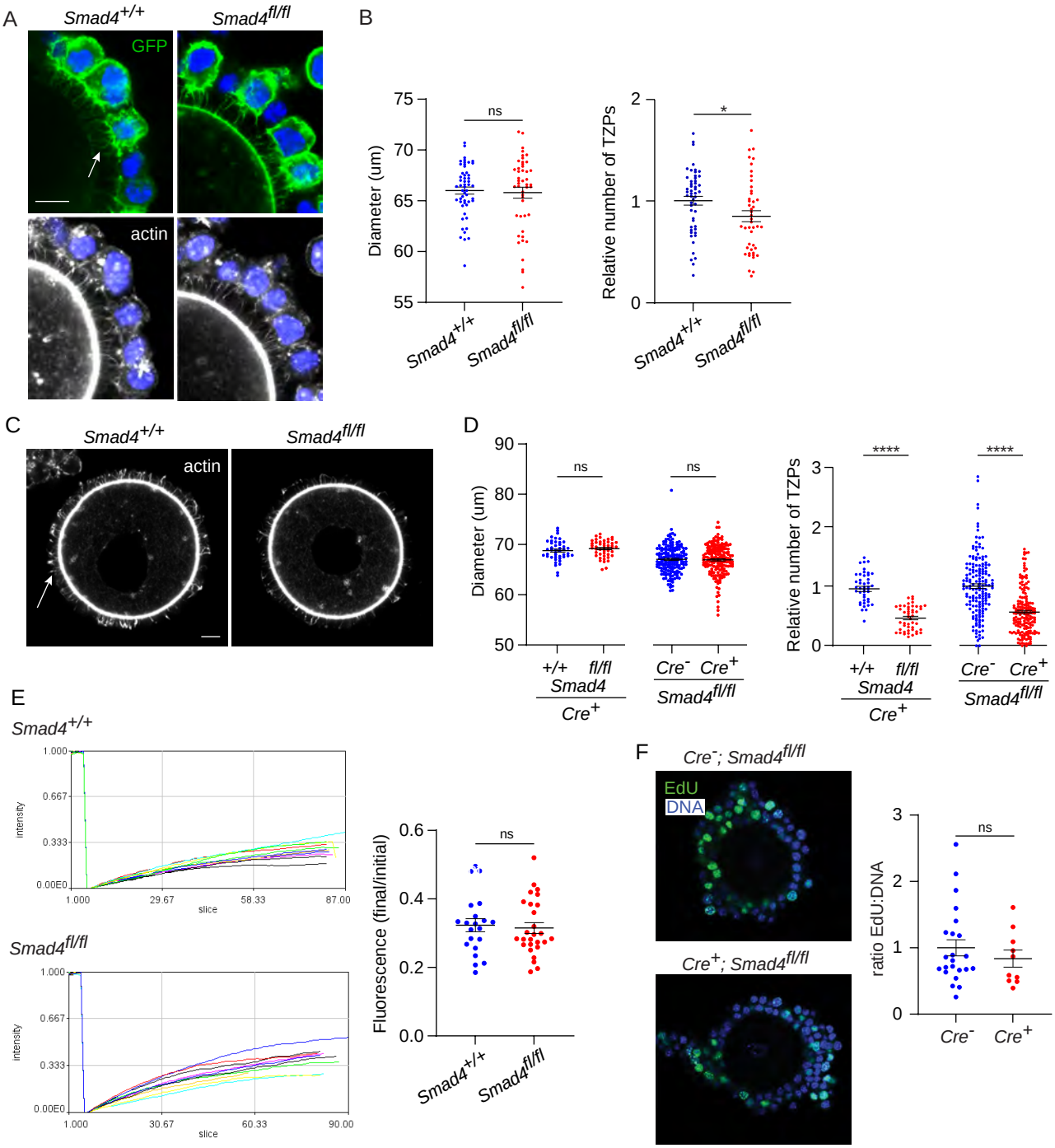
A
Smad4+/+
Smad4fl/fl
GFP
actin
B
Diameter (um)
ns
Relative number of TZPs
*
Smad4+/+
Smad4fl/fl
C
Smad4+/+
Smad4fl/fl
actin
D
Diameter (um)
ns
ns
Relative number of TZPs
****
****
+/+
fl/fl
Smad4
Cre+
Cre-
Cre+
Smad4fl/fl
E
Smad4+/+
intensity
slice
Smad4fl/fl
intensity
slice
Fluorescence (final/initial)
ns
Smad4+/+
Smad4fl/fl
F
Cre-; Smad4fl/fl
EdU
DNA
Cre+; Smad4fl/fl
ratio EdU:DNA
ns
Cre-
Cre+

Figure 3

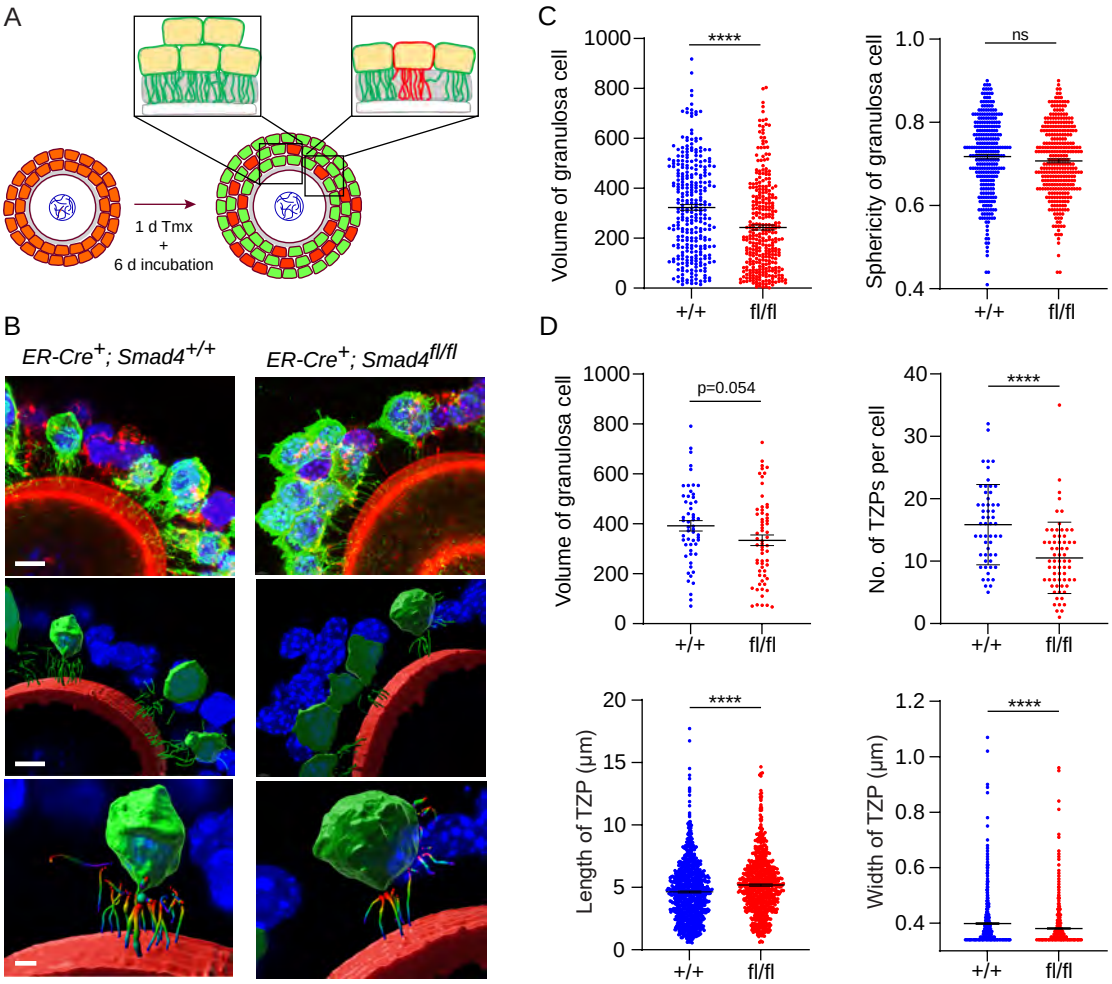
A
1 d Tmx
+
6 d incubation
B
ER-Cre+; Smad4+/+
ER-Cre+; Smad4fl/fl
C
Volume of granulosa cell
****
+/+
fl/fl
Sphericity of granulosa cell
ns
D
Volume of granulosa cell
p=0.054
No. of TZPs per cell
****
Length of TZP (µm)
Width of TZP (µm)

Figure 4

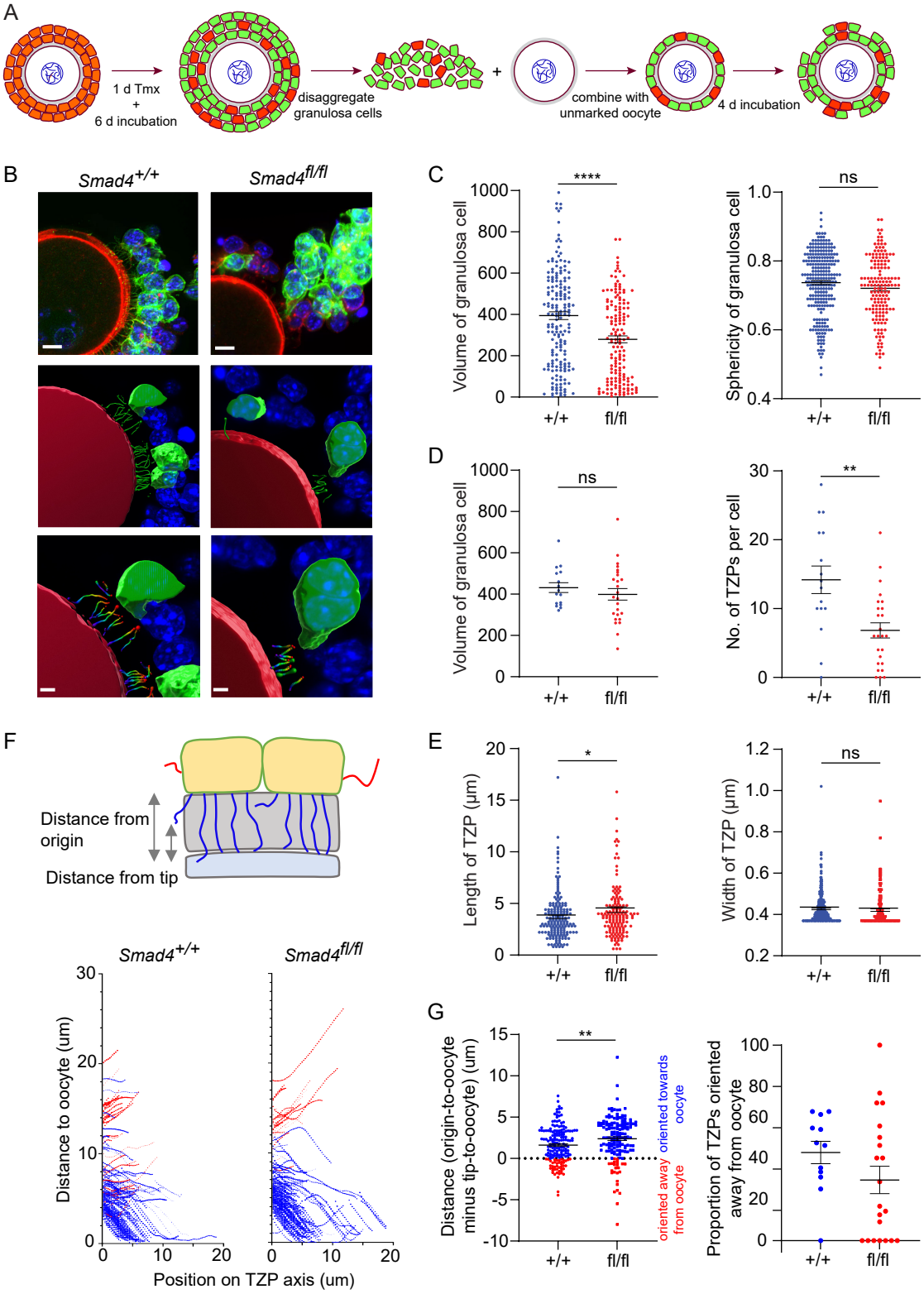
A
1 d Tmx
+
6 d incubation
disaggregate
granulosa cells
+
combine with
unmarked oocyte
4 d incubation
B
Smad4+/+
Smad4fl/fl
C
Volume of granulosa cell
****
Sphericity of granulosa cell
ns
+/+
fl/fl
D
Volume of granulosa cell
ns
No. of TZPs per cell
**
E
Length of TZP (µm)
*
Width of TZP (µm)
ns
F
Distance from
origin
Distance from tip
Smad4+/+
Smad4fl/fl
Distance to oocyte (um)
Position on TZP axis (um)
G
Distance (origin-to-oocyte
minus tip-to-oocyte) (um)
**
oriented towards
oocyte
oriented away
from oocyte
Proportion of TZPs oriented
away from oocyte

Figure 5

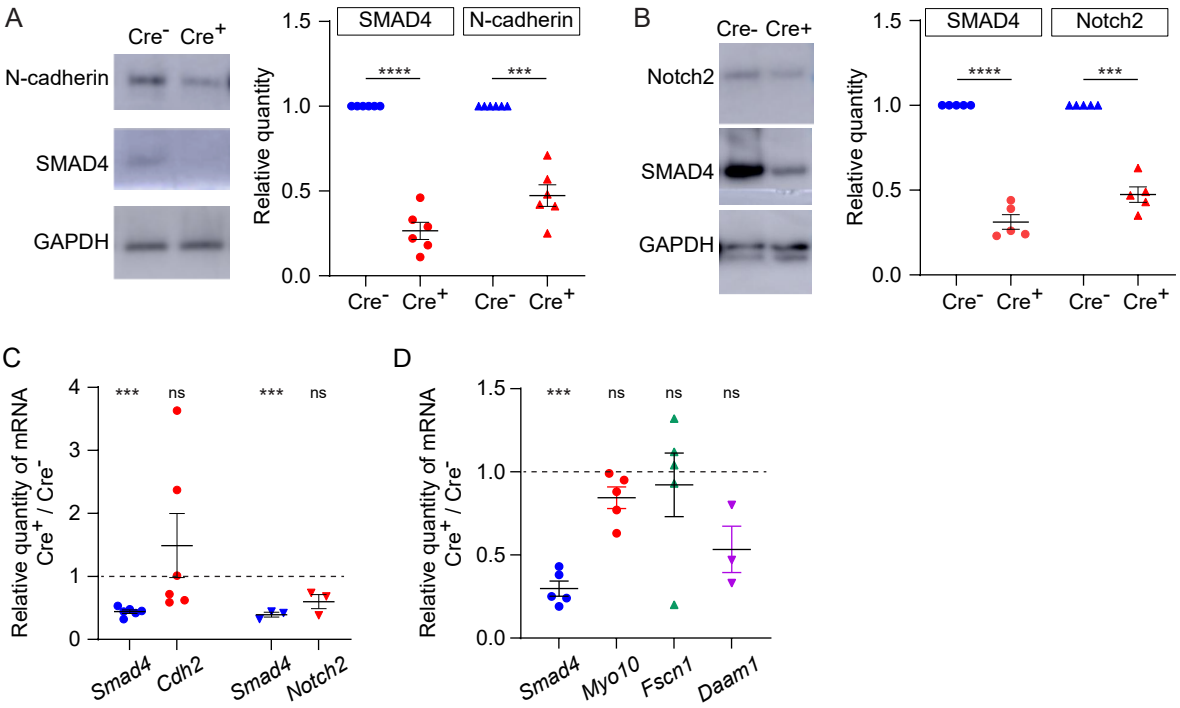
A
Cre⁻ Cre⁺
N-cadherin
SMAD4
GAPDH
SMAD4
N-cadherin
Relative quantity
1.5
1.0
0.5
0.0
****
***
Cre⁻ Cre⁺ Cre⁻ Cre⁺
B
Cre- Cre+
Notch2
SMAD4
GAPDH
SMAD4
Notch2
Relative quantity
****
***
Cre⁻ Cre⁺ Cre⁻ Cre⁺
C
Relative quantity of mRNA Cre⁺ / Cre⁻
4
3
2
1
0
***
ns
***
ns
Smad4
Cdh2
Smad4
Notch2
D
Relative quantity of mRNA Cre⁺ / Cre⁻
1.5
1.0
0.5
0.0
***
ns
ns
ns
Smad4
Myo10
Fscn1
Daam1

Figure 6

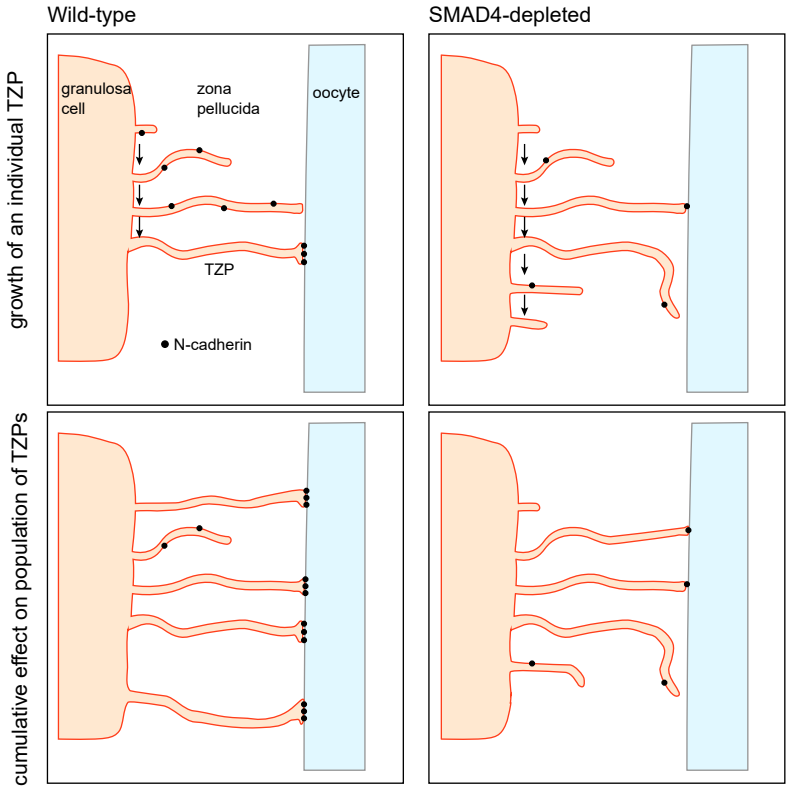
Wild-type
SMAD4-depleted
growth of an individual TZP
cumulative effect on population of TZPs
granulosa cell
zona pellucida
oocyte
TZP
N-cadherin